



# Flexible multibody approaches for simulating the deflection and contact mechanics of toothbrush bristles: modelling and testing

Alessio Cellupica<sup>1</sup> · Luca D'Angelo<sup>1</sup> · Marco Cirelli<sup>1</sup> · Marta Mazur<sup>2</sup> · Pier Paolo Valentini<sup>1</sup>

Received: 15 December 2023 / Accepted: 8 April 2024  
© The Author(s), under exclusive licence to Springer Nature B.V. 2024

## Abstract

Brushing represents a specific procedure that aims to remove biofilms from the vertical and occlusal surfaces of the teeth, as well as from interdental spaces to the greatest extent possible. When developing toothbrushes, a common concern is determining the contact force required to assess cleaning performance, comfort and safety. This evaluation relies on the bristles, which serve as the contact elements of the toothbrush. Due to the significant deflection of the bristles, linear models or two-dimensional approaches may be inadequate for studying their deformation. On the other hand, nonlinear beam models are computationally intensive due to the lack of exact closed-form expressions for large complex deformations. Flexible multibody methodology emerges as a suitable approach to analyse this problem, offering insights into contact forces, sliding forces and bristle deformation. It proves to be a valuable tool for enhancing bristle design. The paper explores two multibody modelling approaches capable of accommodating large deflections. The first is a simplified model based on Howell's PRB 3D model, employing a beam split into two segments connected by a spherical joint and three lumped spring elements. The second is the discrete flexible approach, utilising a larger number of rigid bodies connected with six-degrees-of-freedom elastic matrix elements. Both methods are compared with quantitative experimental results replicating toothbrush cleaning on reference surfaces along different directions.

**Keywords** Flexible multibody · Bristle · Contact mechanics · Pseudo-rigid body · Toothbrush

## 1 Introduction

A relevant topic in dentistry concerns the determination of the forces required for the effective removal of biofilm and plaque from teeth while avoiding damage to soft tissues. The shift from tufts to bristles in the development of toothbrushes has prompted a more in-depth examination within the scientific community regarding the interaction forces between the toothbrush and the teeth. Specifically, the research has focused on assessing the forces applied by the bristles when in contact with a surface. Brushing has been the subject of a thorough examination in the field of periodontology and dental hygiene since the 1960s [1]. The

---

Extended author information available on the last page of the article

effectiveness of brushing is based on empirical data derived from clinical investigations, the standardisation of patients and practices, and the periodic evaluation of toothbrushes [2, 3]. There is a direct correlation between the force applied and the effectiveness of brushing, up to a certain threshold value. Beyond this threshold, the correlation decreases [4]. Mathematical models and in-vitro studies have been employed to characterise the brushing process. Optimal bristle designs have been crafted using mathematical data to ensure maximum therapeutic effectiveness with minimal impact on soft and hard tissues [5–7]. To investigate the performance of tooth brushing, several mathematical models have been studied to evaluate the stiffness of the toothbrush. These models take into account various design variables such as bristle modulus, diameter, length, cross-sectional shape and material [8–10]. Analytical methods, finite-element analysis and flexible multibody techniques have all been applied to examine bristle models for brushing on flat and curved surfaces [11–15]. The pseudo-rigid-body approach was implemented to represent the compliance of the toothbrush tufts, and a thorough comparison of analytical and experimental results has been carried out [16, 17].

These investigations have offered valuable insights into the dynamics of bristle movement, the interactions involving the brush and oral biofilm, enamel, and soft tissue, as well as the effectiveness of different brush configurations in a large variety of other applications such as road sweeping and satellite detumbling [18, 19]. When brushing the teeth, the bristles undergo significant three-dimensional deflection, impacts, jamming, buckling, and other non-linear phenomena owing to the intricate geometry of the teeth, characterised by asperities, tight gaps, and peaks. Due to the elasto-kinematic behaviour of the bristles, which leads to large displacements, and due to the large number of contacts, their non-linear nature and their potential different mechanics [20, 21], studying the deformation of the bristles is not feasible using linear models or two-dimensional approaches. It requires the simulation of complex numerical models, as exact closed-form expressions are not available to address extensive complex deformations [22]. Consequently, a reliable and more comprehensive numerical technique is imperative for calculating quantitative performance metrics and comparing various design solutions or operational scenarios [23–25].

This paper aims to evaluate two pseudo-rigid multibody models [26], one based on Howell's 2D Pseudo-Rigid Body (PRB) concept [20, 21] and the other based on the Discrete Flexible Multibody formulation (DFM) [27–29]. In particular, these modelling techniques are applied to the modern toothbrush made of silicone, as shown in Fig. 1. To effectively compare the two approaches, depicted in Fig. 2, the study focuses on the evaluation of the tangential and normal contact forces that occur when the toothbrush's bristles interact with a flat surface. Furthermore, to estimate the actual bristle deformation and contact forces, an experimental setup is built, and the results are compared with those of the multibody models. The paper is structured as follows: the initial section outlines the problem definition, emphasising the hypotheses and boundary conditions that form the basis for the development of different models. Subsequently, the multibody models are detailed, along with their application to the toothbrush. The next section describes the experimental assembly, highlighting the accuracy of data acquisition. In the concluding part, the outcomes related to bristle deformation and contact forces from multibody models are presented and then compared with the results obtained from the experimental setup.

## 2 Multibody models and methodologies

The initial phase of this study consists of explaining the multibody models employed for evaluating the deformation and the contact forces acting on the bristles. The first multibody

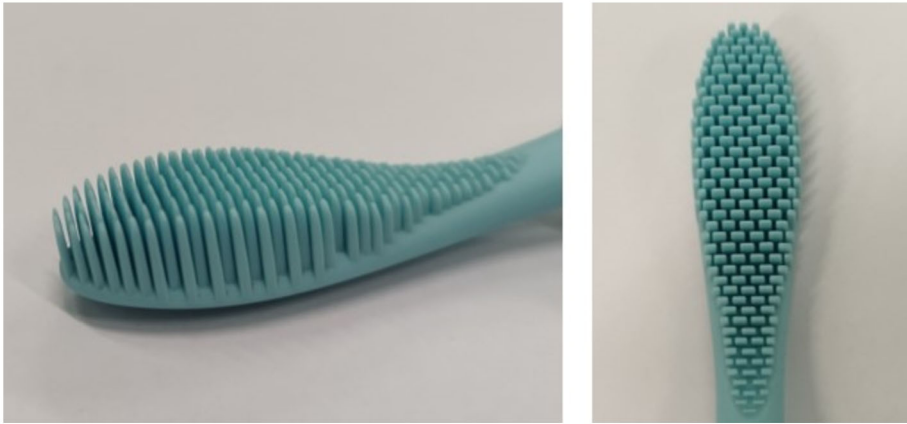


**Fig. 1** The modern toothbrush of the current investigation: on the left, a perspective view showing the complex geometry of the bristles; on the right, the top view

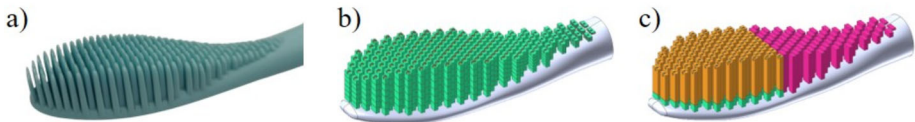


**Fig. 2** Comparison of the prospective views of the toothbrush. a) actual toothbrush; b) DFM model; c) Howell PRB model

model is based on an extension of the Howell bidimensional pseudo-rigid-beam approach to the 3D space [20, 21, 30]. Following the Howell approach, each bristle was split into two segments connected by a spherical joint and a lumped torsional spring element. The second one is the discrete flexible multibody (DFM) technique [27–29], which is based on a regular but more detailed discretisation with rigid bodies connected by elastic six-degrees-of-freedom lumped elements (stiffness matrices) [31, 32].

## 2.1 Multibody model based on Howell's PRBM

In the 2D Howell approach, the bristle is conceptualised as a flexible cantilever beam with a constant cross section and linear material properties, subjected to an end-tip load. When the deflection increases, the linearised beam deflection theory loses validity. The pseudo-rigid-body model of the flexible beam provides a simple but sufficiently accurate approach to analysing deflections. For a flexible cantilever beam with a force applied at the free end, elliptic-integral equations for large deflections reveal that the free end traces an approximately circular path. Using this insight, Howell devises a pseudo-rigid model where this circular path can be precisely represented by two rigid links connected at a pivot along the beam (Figure 3a). A torsional spring at the pivot models and collects the beam's resistance to deflection. The position of this characteristic pivot in the pseudo-rigid body is expressed as a fraction of the length of the beam, denoted by  $\gamma l$  with  $\gamma$  representing the characteristic radius factor [20]. The coefficient  $\gamma$  can be deduced from the ratio:

$$n = \frac{F_n}{F_t}. \quad (1)$$

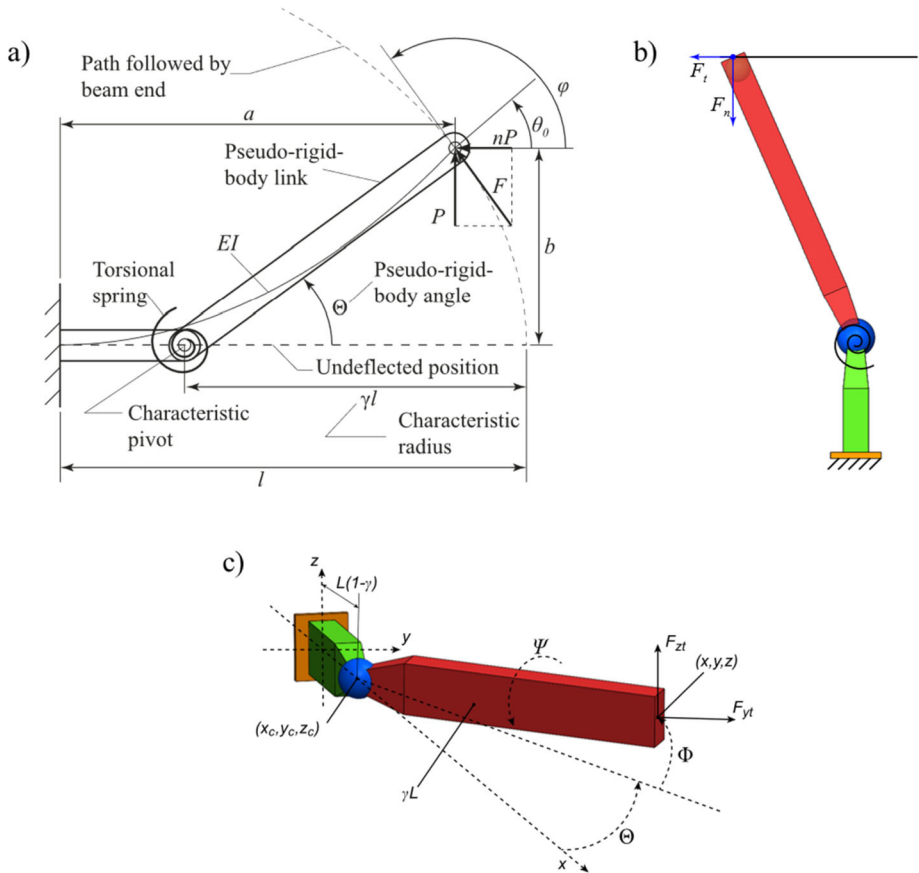


**Fig. 3** a) Cantilever beam with forces at the free end and its pseudo-rigid-body model according to Howell. b) Application of the PRB model to the toothbrush contacting a flat surface. c) The generalised Howell's 3D PRB model

Considering the contact of the beam end with a flat surface (Figure 3b),  $F_n$  and  $F_t$  may be reviewed as the normal and tangential contact forces, respectively. Therefore, assuming a Coulomb friction model [33], the term  $n$  is the reciprocal of the friction coefficient  $\mu$  for the specific contact configuration:

$$n = \frac{1}{\mu}. \tag{2}$$

Once  $n$  is known, it is possible to use Table 1, derived by Howell [20], to compute  $\gamma$  and, consequently, the coefficient  $K_\Theta$ , which is the characteristic stiffness parameter of the PRB model.

From these coefficients, it is possible to compute the revolute joint position  $\gamma l$  and the torsional spring stiffness  $k$  as follows:

$$k = \gamma K_\Theta \frac{EI}{l}. \tag{3}$$

**Table 1** Numerical data for  $n$ ,  $\gamma$ ,  $K_\Theta$  [20]

$n$	$\gamma$	$K_\Theta$
0.0	0.8517	2.67617
0.5	0.8430	2.63744
1.0	0.8360	2.61259
1.5	0.8311	2.59289
2.0	0.8276	2.59707
3.0	0.8232	2.56737
4.0	0.8207	2.56506
5.0	0.8192	2.56251
7.5	0.8168	2.55984
10.0	0.8156	2.56597

The parameter  $E$  is the Young’s modulus of the bristle,  $I$  is the inertia modulus of the cross section of the bristle with respect to the direction of the inflection plane, and  $l$  is the bristle length.

In order to extend this bidimensional formulation to the 3D case (Figure 3c), the Howell 2D PRB model approach is applied to the two main deflection planes of the bristles. In a previous study [30], it has been shown that the 3D beam end’s pathway will slightly deform into an ellipsoidal shape for large displacements. However, the extended PRB model used in this work assumes that the mixed inflection contributions are negligible, due to the similar cross-sectional dimensions. For this reason, the expected path of the beam end is assumed to lie on a spherical surface. Two torsion springs acting on the two main bending directions  $y$  and  $z$  are included. Their stiffness is computed as:

$$\begin{aligned} k_y &= \gamma K_\Theta \frac{EI_y}{l} \\ k_z &= \gamma K_\Theta \frac{EI_z}{l} \end{aligned} \tag{4}$$

where  $E$  is the Young’s modulus and  $I_y$  and  $I_z$  are the moments of inertia with respect to the two bending directions, respectively.

Another torsion spring is added to take into account the torsion stiffness:

$$k_x = \frac{GJ_x}{\gamma l}, \tag{5}$$

where  $G$  is the shear modulus and  $J_x$  is the polar moment of inertia with respect to the torsion axis  $x$ . Inspired by the Howell formulation, this multibody model is generated by splitting the bristle according to the parameters reported in Table 1 and applying a spherical joint as a connection. On this joint, a lumped three-dimensional stiffness-damping element is applied. The stiffness matrix is computed by combining equations (4) and (5) as follows:

$$\mathbf{K} = \begin{bmatrix} \frac{GJ_x}{\gamma l} & 0 & 0 \\ 0 & \gamma K_\Theta \frac{EI_y}{l} & 0 \\ 0 & 0 & \gamma K_\Theta \frac{EI_z}{l} \end{bmatrix}. \tag{6}$$

The damping matrix is introduced in the following form:

$$\mathbf{C} = \begin{bmatrix} c_1 & 0 & 0 \\ 0 & c_2 & 0 \\ 0 & 0 & c_3 \end{bmatrix}. \tag{7}$$

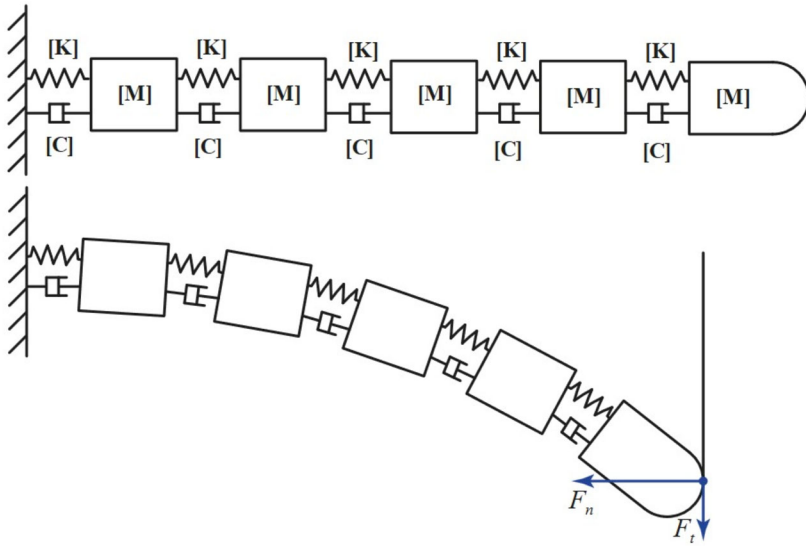


Fig. 4 The discrete rigid-body model of a bristle

Finally, the force vector  $\mathbf{F}$  and the displacement vector  $\mathbf{\Delta}$  are connected by the following formula:

$$\mathbf{F} = \mathbf{K}\mathbf{\Delta} + \mathbf{C}\dot{\mathbf{\Delta}} \tag{8}$$

### 2.2 Discrete Flexible Multibody model (DFM)

Although the fundamental concept of the DFM model shares similarities with the PRB model, the DFM should offer a more detailed description of structural deflection and contact mechanics due to its specific implementation. In the DFM methodology, the bristle is discretised into multiple nodes, as illustrated in Fig. 4, with each node possessing six degrees-of-freedom, mass and inertia (referred to as rigid-body nodes).

The interaction between adjacent nodes is preserved through stiffness matrices, generating reaction forces and moments based on the relative displacement between the coordinate reference systems of adjacent nodes. Conceptually, these stiffness matrices produce a  $6 \times 6$  force field, activating upon any relative displacement. The Timoshenko beam theory is applied to deduce the general stiffness matrix acting between two nodes [28]:

$$\mathbf{K}_{i,i+1} = \begin{bmatrix} \frac{EA}{L} & 0 & 0 & 0 & 0 & 0 \\ 0 & \frac{12EI_{zz}}{L^3(1+P_y)} & 0 & 0 & 0 & \frac{-6EI_{xy}}{L^2(1+P_y)} \\ 0 & 0 & \frac{12EI_{yy}}{L^3(1+P_z)} & 0 & \frac{6EI_{yx}}{L^2(1+P_z)} & 0 \\ 0 & 0 & 0 & \frac{GI_{xy}}{L} & 0 & 0 \\ 0 & 0 & \frac{6EI_{yy}}{L^2(1+P_z)} & 0 & \frac{(4+P_z)EI_{yy}}{L(1+P_z)} & 0 \\ 0 & \frac{-6EI_{xy}}{L^2(1+P_y)} & 0 & 0 & 0 & \frac{(4+P_y)EI_{zz}}{L(1+P_y)} \end{bmatrix}, \tag{9}$$

where

$$P_y = \frac{12EI_{zz}A_{sy}}{GAL^2} \tag{10}$$

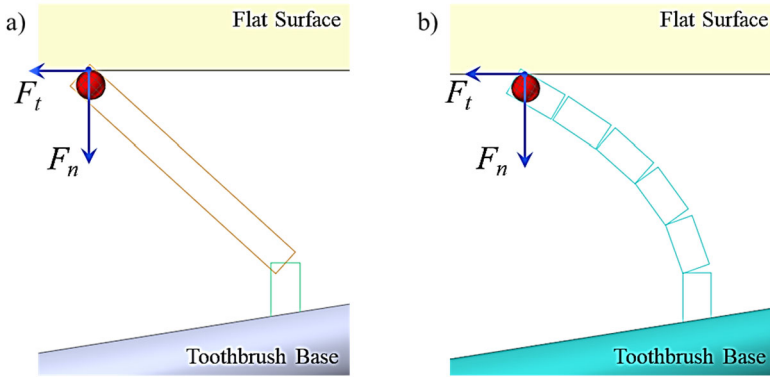


Fig. 5 Contact between a bristle and the flat surface for a) Howell PRB model and b) DFM model

$$P_z = \frac{12EI_{yy}A_{sz}}{GAL^2}, \tag{11}$$

where  $A_s$  is the shear area ratio,  $E$  is the Young’s Modulus,  $G$  is the shear modulus,  $A$  is the section area,  $L$  is the distance between adjacent nodes and  $I_{jj}$  is the moment of inertia of the cross section about the  $j$ -axis.

Moreover, each damping matrix can be defined as follows:

$$C_{i,i+1} = \begin{bmatrix} c_{11} & \cdots & c_{16} \\ & \ddots & \vdots \\ Sym & & c_{66} \end{bmatrix}. \tag{12}$$

As a result, the forces and moments exchanged by adjacent nodes can be expressed as:

$$F_{i,i+1} = K_{i,i+1}\Delta_{i,i+1} + C_{i,i+1}\dot{\Delta}_{i,i+1}, \tag{13}$$

where  $\Delta_{i+1,i}$  and  $\dot{\Delta}_{i+1,i}$  are the vector of relative displacements (translational and rotational) and relative velocity between the nodes’ generalised coordinates, respectively.

The number of discretised elements may be chosen depending on the complexity of the deformation and the required accuracy.

### 2.3 Contact model

The contact between each bristle and the flat surface is detected between a sphere fixed to the end of the beam and a flat plane (Fig. 5).

The introduction of these auxiliary bodies simplifies the contact computation and increases the robustness of detection thanks to the use of the analytical equation for sphere-to-plane contact. Given the large number of points in contact, the use of the sphere-to-plane contact is necessary to reduce the computational burden [34]. To efficiently identify contact points, a systematic detection method is necessary. The search algorithm is structured around a preliminary search for contact zones followed by a refined search for the contact-region penetration depth. The force generated at each contact point is computed with a penalty formulation (Eq. (14)), based on the Hertz theory [35, 36], and extended by Flores [37]. The

contact formulation [34, 38] allows calculation of the normal force through the relation:

$$F_n = k\delta^{m_1} + c\frac{\dot{\delta}}{|\dot{\delta}|}|\dot{\delta}|^{m_2}\delta^{m_3}, \quad (14)$$

where:

- $\delta, \dot{\delta}$  are the penetration and its speed;
- $m_1, m_2$  and  $m_3$  are the exponents of stiffness, damping and indentation factor, respectively;
- $k$  and  $c$  are the stiffness and damping coefficients.

To compute the tangential contact force a velocity-based friction model is adopted [39–42]. It is computed by multiplying the normal component by the friction coefficient (that depends on the sliding velocity) and applied along the direction opposite to that of the sliding velocity at the contact point:

$$F_t = -|\mu(v_t)|F_n\frac{v_t}{\|v_t\|}, \quad (15)$$

where  $v_t$  is the relative sliding velocity at the contact point (perpendicular to the normal vector). The friction coefficient  $\mu(v_t)$  depends on the static friction coefficient ( $\mu_s$ ), the dynamic friction coefficient ( $\mu_d$ ), the dynamic velocity tolerance ( $v_d$ ) and the static velocity tolerance ( $v_s$ ). Although this model is not able to take into account stiction, it is capable of implementing a smooth transition between static friction and dynamic friction.

Internal contact between bristles is intentionally neglected to reduce computational complexity. However, recognising the significance of this contribution is crucial to a comprehensive understanding of the problem. Specifically, in scenarios where the direction of motion varies, the interaction among bristles may become important. This interaction may result in a decrease in normal forces as the bristles establish internal contact, thus exerting a diminished pressure on the flat surface. However, the validity of this assumption is then verified against experiment, as discussed in the next sections of the paper.

## 2.4 Equations of motion

The equations of motion of the generic rigid-body node for both methods can be written as follows:

$$\mathbf{M}_i\ddot{\mathbf{q}}_i + \mathbf{K}_{i,i-1}\Delta_{i,i-1} - \mathbf{K}_{i,i+1}\Delta_{i,i+1} + \mathbf{C}_{i,i-1}\dot{\Delta}_{i,i-1} - \mathbf{C}_{i,i+1}\dot{\Delta}_{i,i+1} = \mathbf{F}_{n,i} + \mathbf{F}_{t,i}, \quad (16)$$

where:

$$\mathbf{M}_i \text{ is the mass matrix, } i.e. \mathbf{M}_i = \frac{\rho\pi\phi^2L}{4} \begin{bmatrix} 1 & 0 & 0 & 0 & 0 & 0 \\ 0 & 1 & 0 & 0 & 0 & 0 \\ 0 & 0 & 1 & 0 & 0 & 0 \\ 0 & 0 & 0 & \frac{\phi^2}{8} & 0 & 0 \\ 0 & 0 & 0 & 0 & \frac{\phi^2}{16} + \frac{L^2}{12} & 0 \\ 0 & 0 & 0 & 0 & 0 & \frac{\phi^2}{16} + \frac{L^2}{12} \end{bmatrix},$$

$\ddot{\mathbf{q}}_i$  is the vector of the generalised acceleration ( $\ddot{\mathbf{q}}_i = \frac{d^2\mathbf{q}_i}{dt^2}$ );



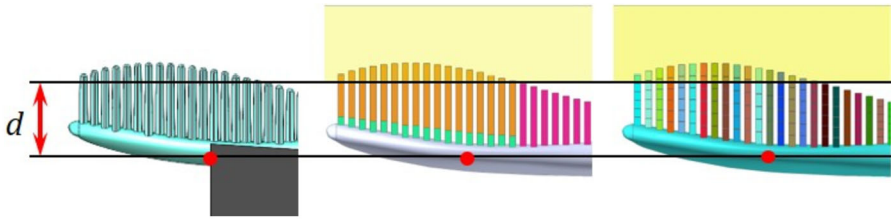


**Fig. 6** Initial conditions of the simulated scenario with the highlight on the interaction distance between the toothbrush handle and the flat surface

$\mathbf{K}_{i,i-1}$  and  $\mathbf{K}_{i,i+1}$  are the stiffness matrices of the elastic compliance between node  $i$  and nodes  $i - 1$  and  $i + 1$ , respectively;

$\mathbf{C}_{i,i-1}$  and  $\mathbf{C}_{i,i+1}$  are the damping matrices between node  $i$  and nodes  $i - 1$  and  $i + 1$ , respectively;

$\Delta_{i,i-1} = \mathbf{q}_{i-1} - \mathbf{q}_i$  and  $\Delta_{i,i+1} = \mathbf{q}_{i+1} - \mathbf{q}_i$  are the relative displacement between nodes  $i$  and nodes  $i - 1$  and  $i + 1$  generalised coordinates, respectively.

$\mathbf{F}_{n,i}$  and  $\mathbf{F}_{t,i}$  are the contact loads at each adjacent nodes' connections.

### 3 Case study

The described modelling approaches are tested on a simulation of a toothbrush head bushing on a flat surface along the two main directions and then compared against experimental tests. The mathematical models are based on several assumptions. Actually, in both the developed models, a considerable number of variables are involved. For this reason, the following simplifying hypotheses are introduced to reduce the computational complexity:

- the cross section of the toothbrush bristles is assumed to be rectangular and constant along the midline of the bristle;
- the deformation of the flat surface is neglected, assuming it to be infinitely rigid;
- the toothbrush support (i.e., handle) in the experimental setup is treated as undeformable;
- the multibody models neglect the influence of mutual interaction among the bristles, as discussed in the previous section.

The toothbrush is made of silicone with a Young's modulus ( $E$ ) of 7.5 MPa, the interacting surface is made of acrylic and the friction coefficient is assumed to be  $\mu_d = 0.76$ , after some preliminary tests. Each bristle terminates with a sphere of 0.4 mm of radius that may interact with the flat plane. The reference interaction distance  $d$  between the toothbrush and the plane (see Fig. 6) is set at 4.2 mm.

Referring to the handle of the toothbrush, the interaction forces were examined in two different scenarios: brushing in the orthogonal direction (see Figure 7a) and brushing in the parallel direction (see Figure 7c). In both cases, the toothbrush is firmly mounted on a slider, driven by a motorised screw that imposes a sinusoidal motion, as shown in Figure 7b and Figure 7d, respectively. For the orthogonal motion, the amplitude is set to 15 mm, whereas for the parallel one, it is 30 mm. Concerning frequency, the first case adopts  $\pi/6$  rad/s, while the second case uses  $\pi/12$  rad/s.

Considering the PRB model, the computation of the Howell factors from Table 1, considering a linear interpolation, yields  $\gamma = 0.8329$  and  $K_{\ominus} = 2.6001$ . In the DFM model, each bristle is discretised with six rigid bodies. The parameters used in the contact formulation (Eq. (14)) are summarised in the Table 2.

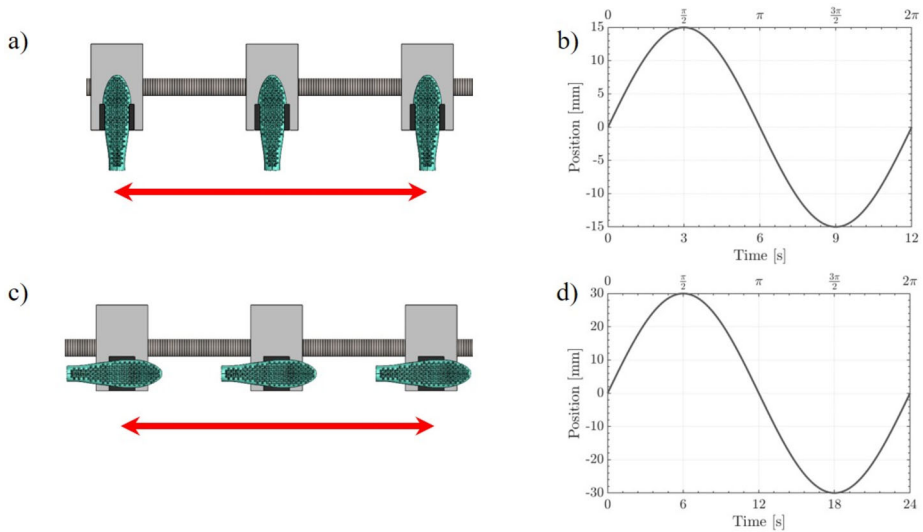


**Fig. 7** Periodic motion applied to the toothbrush: a) motion along the orthogonal brushing direction; b) time history of the motion law for the orthogonal brushing; c) motion along the parallel brushing direction; d) time history of the motion law for the parallel brushing

**Table 2** Parameters adopted for the computation of normal and tangential forces

Parameters for normal force			Parameters for tangential force		
Coefficient	Value	UoM	Coefficient	Value	UoM
$k$	100	N/mm	$\mu_s$	0.8	
$m_1$	1.3		$\mu_d$	0.76	
$c$	0.2	N s/mm	$v_s$	1.2	mm/s
$m_2$	1		$v_d$	1.5	mm/s
$m_3$	2				

## 4 Experimental setup

The purpose of the experimental setup (Figure 8a) is to acquire the forces acting on the toothbrush along the normal and tangential directions for a quantitative comparison. Moreover, the assessment of the deformation is accomplished by a simplified visual inspection using a camera.

The toothbrush is securely connected to a support that can slide attached to a ball screw driven by a motor. For visualising the physical deformation of the bristles, a fixed Nulaxy Webcam Full HD 1080p is mounted on the frame. The experimental setup is built using a 12 V, 10 A power supply, a NEMA23 ST57H703 stepper motor, a TB6600 Stepper Motor Driver, two Arduino Mega 2560 boards, two extensimetric load cells with weight range between 0–1 kg and two HX711 A/D Modules. A flat transparent acrylic surface is mounted on an adjustable frame above the slider. One Arduino board manages the movement of the two-phase bipolar stepper motor, and the other simultaneously acquires the data from the load cells. The two load cells are mounted between the slider and the toothbrush, assessing forces along two orthogonal directions. Figure 8b and Figure 8c show the interconnection

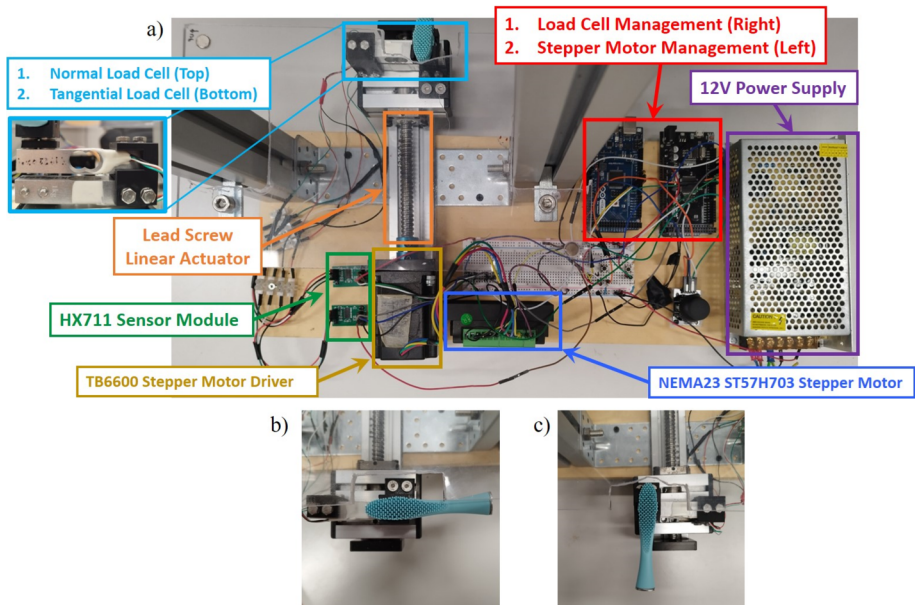


**Fig. 8** a) Complete experimental bench. b) Orthogonal and c) parallel brushing toothbrush grabbing and movement setup

system among the toothbrush, load cells and slider for orthogonal and parallel brushing, respectively.

## 5 Results and discussion

The comparative analysis between the two models and the experimental investigation is conducted through a dual approach: first, by a qualitative visual inspection of the bristle deformation, and secondly, by the quantitative comparison of the normal and tangential reaction forces, examined at the base of the toothbrush.

**Visual inspection** Figure 9 and Fig. 10 show the deformation of the bristles, during brushing in the orthogonal and parallel directions, respectively, for a quick visual comparison of the results. Concerning orthogonal brushing, Figures 9a, 9b, 9g, 9h, 9o and 9p illustrate the motion frames from top to bottom, where the deflection of the bristles follows the direction of brushing motion. Figures 9e, 9f, 9m, 9n, 9s and 9t show the deformation of the bristles when the driving motion changes direction, the inversion of motion occurs, and a snap-through buckling happens. This phenomenon occurs because during the inversion of motion, the friction force inverts its sign and assumes an unstable configuration that tends to stabilise later, changing the curvature of the neutral axis of the bristle. Figures 9c, 9d, 9i, 9l, 9q and 9r present the return from bottom to top. Similarly, for parallel brushing, Figures 10a, 10b, 10g, 10h, 10o and 10p capture the toothbrush's directional motion from right to left. Figures 10e, 10f, 10m, 10n, 10s and 10t show the buckling of the bristles in response to directional motion changes, while Figures 10c, 10d, 10i, 10l, 10q and 10r illustrate the toothbrush's return from left to right. Additionally, Figures 10f, 10n and 10t show bristle jamming and the double-curvature deformation at the beginning of the inversion phase for parallel brushing.

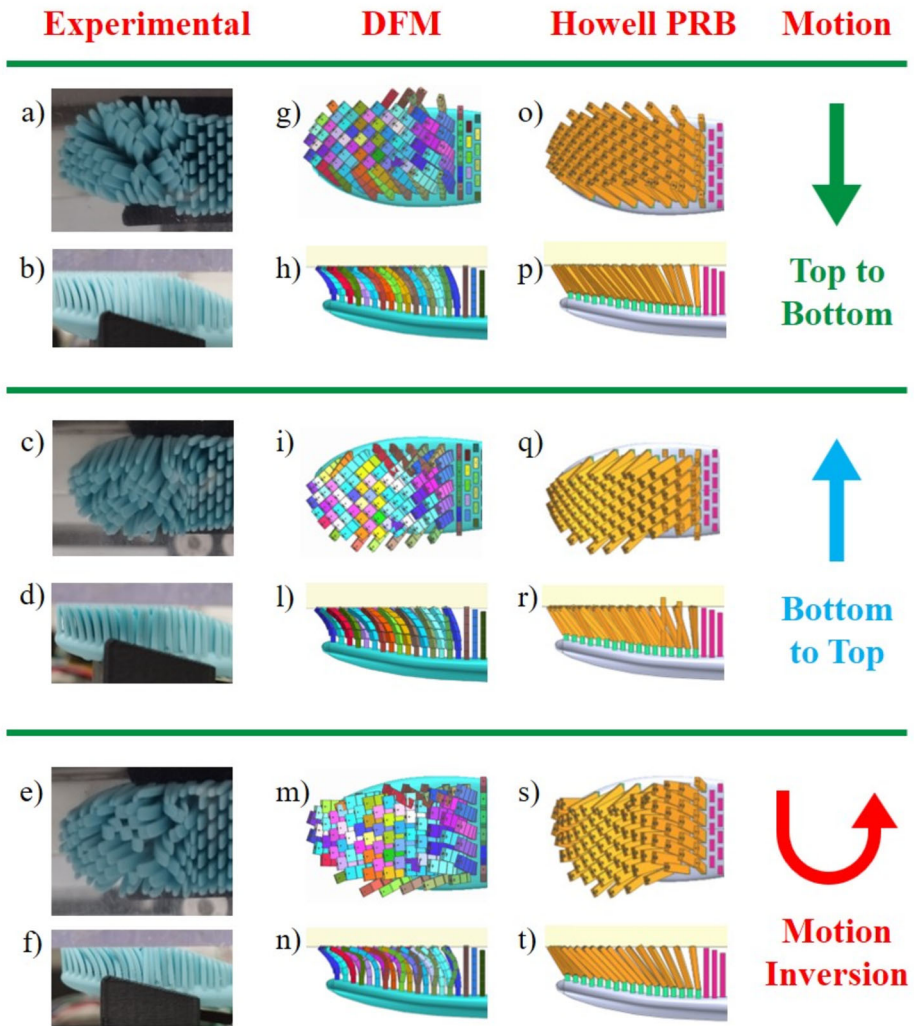


**Fig. 9** Visualisation of the frames for the actual toothbrush (first column), DFM (second column) and PRB model (third column) during the orthogonal motion brushing

As is evident, the DFM model exhibits a potential capability to depict the deformations of the physical bristles, with the limitation that the absence of contact between the bristles introduces a minor discrepancy in the physical results. On the contrary, the PRBM does not closely align with the physical model in terms of bristle deformation for evident reasons. In terms of deformation, the pseudo-rigid-body link in the PRBM lacks the degrees of freedom for deformation, as defined by the discrete multibody model. Consequently, the PRBM cannot adequately represent and address buckling phenomena, primarily because its discretisation is based on two rigid bodies instead of multiple ones; some loss of contact between the bristles and the interaction surface may occur during the incipient buckling phases due to excessive penetration. An example of this contact loss is discernible for some bristles in Figure 9r, which represents brushing after the reversal of motion. However, it is crucial to

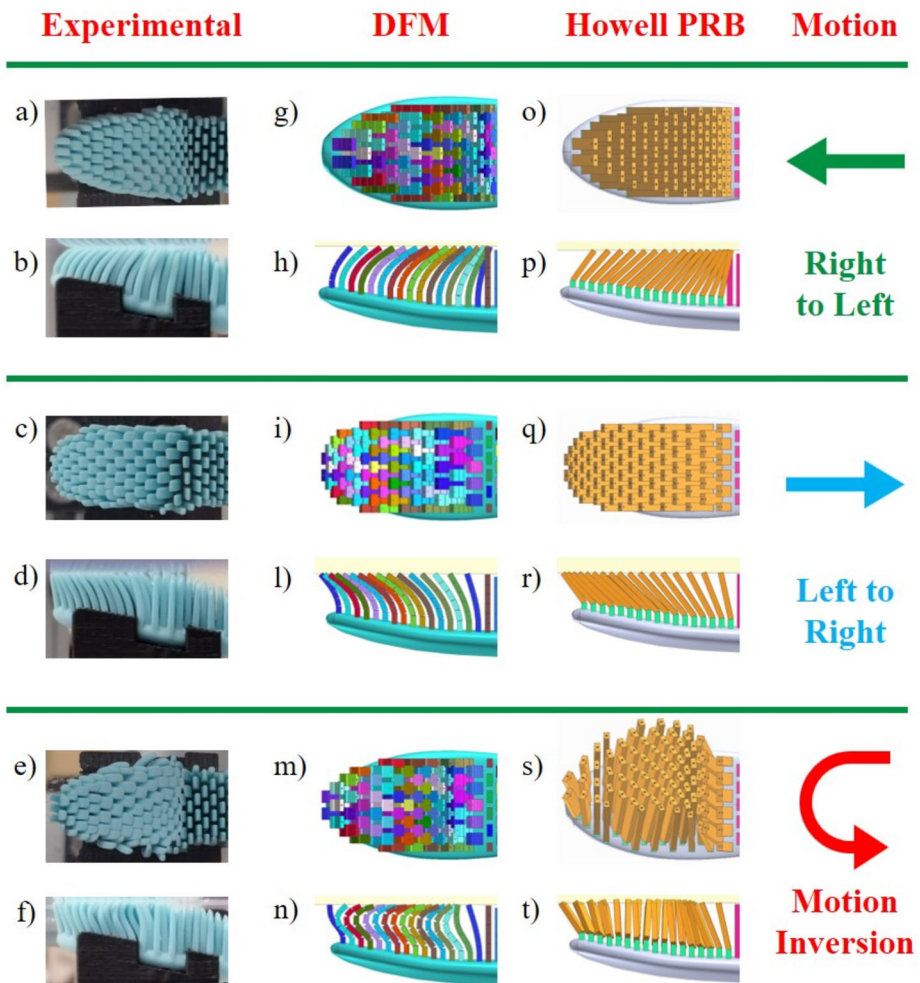


**Fig. 10** Visualisation of the frames for the actual toothbrush (first column), DFM (second column) and PRB model (third column) during the parallel motion brushing

note that the primary focus in toothbrushing lies in evaluating the forces applied by the user to the teeth rather than the deformation of the bristles themselves.

**Load comparison** Figure 11 and Fig. 12 compare the results obtained from DFM, PRBM and the experiments, respectively, in terms of normal force and tangential force for orthogonal brushing.

In general, the figures exhibit two discernible zones: a peak region and an almost flat region. The peaks correspond to the inversion of motion and thus the incipient buckling condition, while the flat region aligns with effective brushing. By analysing Figure 11a, the first two peaks (around 15 mm and 45 mm are amplified with respect to the other. This phenomenon occurs because the bristles had not already reached the stable configuration with a lower energy state in the first two inversions of motions. The configuration of lower energy occurs when the bristles undergo out-of-plane deformation, as illustrated in Figures



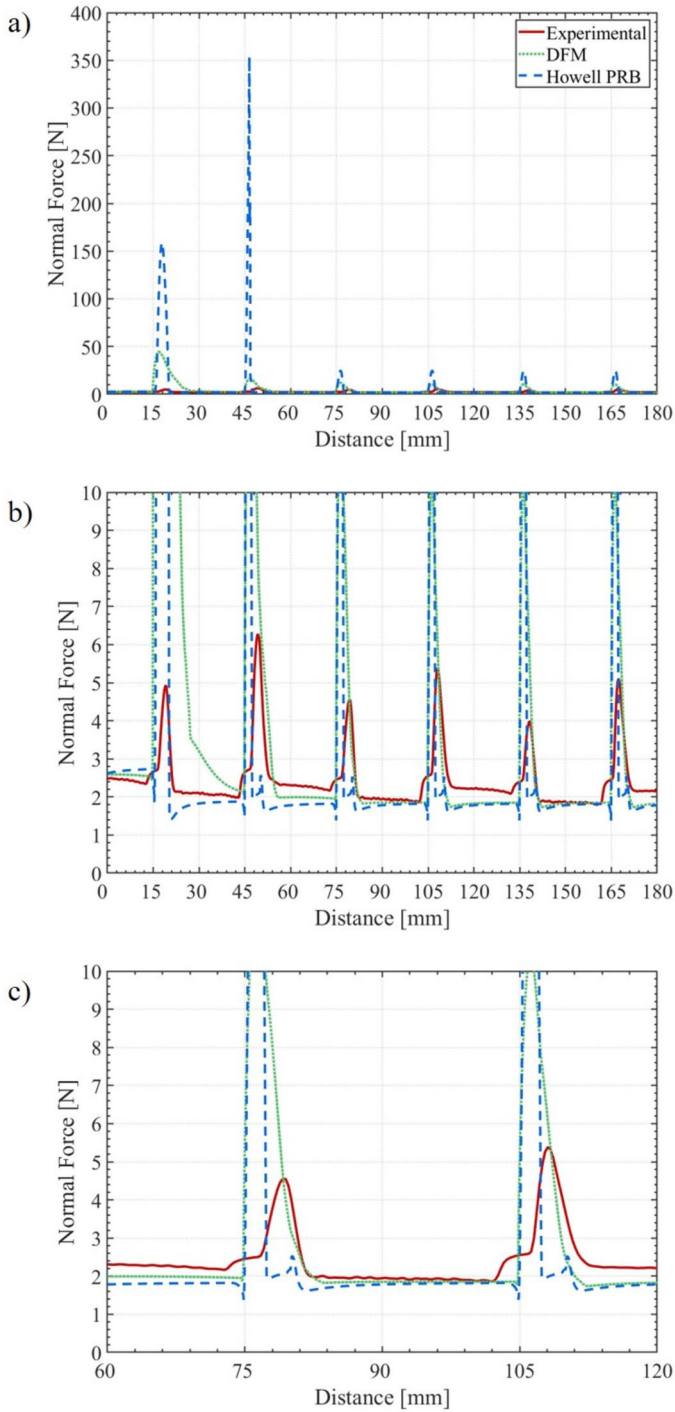


**Fig. 11** a) Comparison of the results obtained for the normal force in the orthogonal brushing; b) comparison zooming along the y-axis; c) comparison on a single motion period

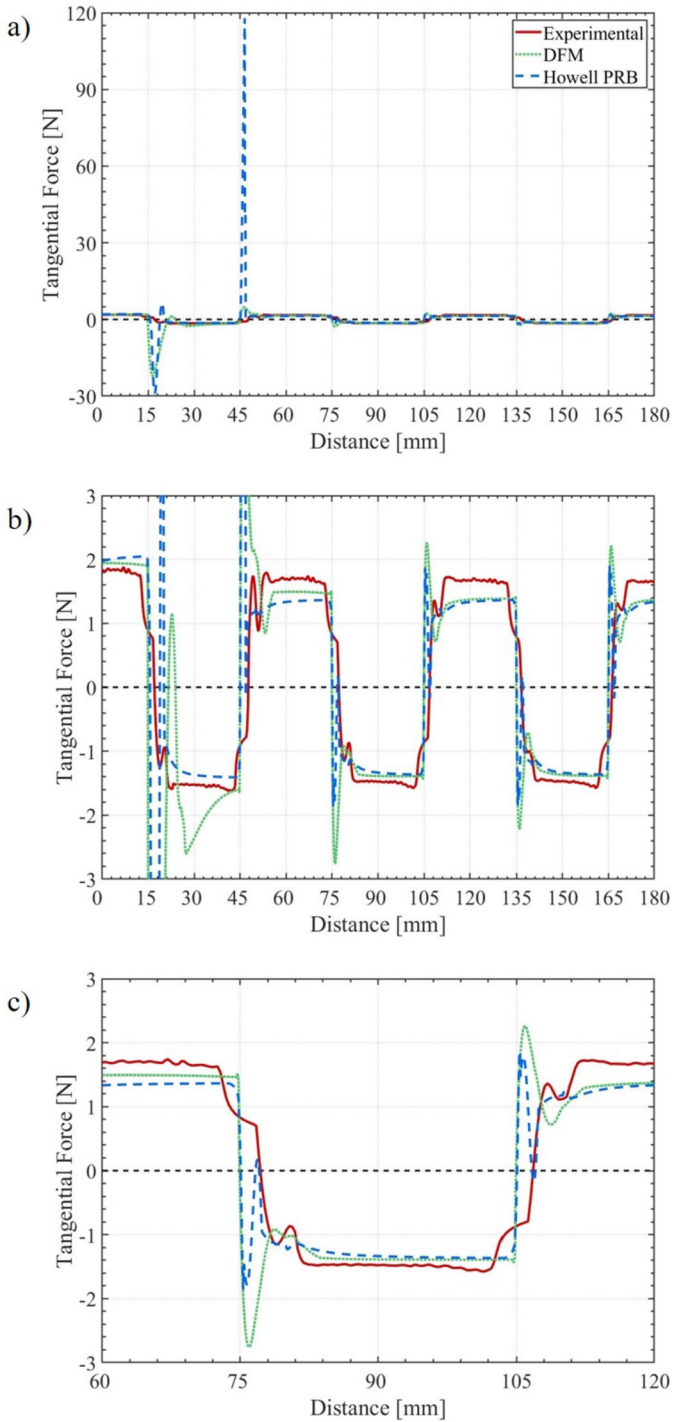


**Fig. 12** a) Comparison of the results obtained for the tangential force in the orthogonal brushing; b) comparison zooming along the y-axis; c) comparison on a single motion period

9g and 9i. While the PRBM needs two inversions of motion to reach the configuration with a lower energy state because of its difficulty to resolve the buckling of the bristles, the DFM needs only one. In Figure 11b, it is possible to observe that the first peak of the DFM is larger than the first peak of PRBM due to the greater number of rigid bodies. Indeed, in the DFM model, a discontinuity of the derivative of both forces is observed near 27 mm of travelled distance, marking the transition between these two configurations. The experimental result does not exhibit this behaviour because the mutual contact among the bristles brings the system in the minimum-energy configuration in a shorter travelling space.

About the PRBM results, a force peak at 45 mm occurs due to reaching the maximum penetration limit for a group of bristles. It is evident in Figure 9q that for a group of bristles, the inability to cope with elastic buckling leads to jamming and to the loss of contact detection. In the subsequent inversions of motion, the peaks of the normal force remain greater for the PRBM than for the experimental case and the DFM, due to the higher stiffness of the rigid-body link: the normal force peaks are twice that of the DFM and four times that of the experimental results. Observing Figure 11b during the brushing phase, the normal forces exhibit small differences in the experimental acquisitions, depending on the direction of motion. These differences may be due to the lack of perfect symmetry of the arrangement. The differences in normal force observed in the effective brushing zone (far from the inversions) between the experimental and PRBM reaches a maximum of approximately 18%. Similarly, when comparing the experimental and the DFM results, the maximum difference in the normal force is 16%. Tangential forces show similar differences since they are linked to the normal ones (see Eq. (15)). It should be noted that, as seen in Fig. 12, during the inversion of motion preceding the effective brushing phase (characterised by approximately constant force), all the models show oscillation in tangential forces due to the dynamic stabilisation of the deformation.

The results obtained from the DFM, PRBM and the experiments, in terms of normal force and tangential force for parallel brushing are reported in Fig. 13 and Fig. 14, respectively.

Examining parallel brushing, in all models, it is evident that the bristles are inherently positioned in a state of minimal-energy configuration. Indeed, there are no noticeable force peaks during the initial motion inversion. This phenomenon arises because of the tendency of the bristle to bend in the direction of the minimal stiffness. In this scenario, the contact detection of the PRBM is always correctly computed also due to the reduced bending stiffness of the bristles about the orthogonal axis of movement and the reduced jamming tendency. The difference between the normal forces during the brushing between the experimental tests and PRBM models is approximately 16%. The difference between the experimental and DFM models is consistently below 8%.

Similarly to orthogonal brushing, parallel brushing also shows an oscillating trend of the tangential force near the motion inversion due to the dynamic stabilisation of the deformation. The experimental differences on the brushing forces depending on motion direction highlighted for the orthogonal scenario are reduced in this case. As highlighted for the orthogonal brushing, even in this scenario the toothbrush shows a smoother transition during motion inversion, as testified by shorter and smaller force peaks during inversions.

As a general comment for both orthogonal and parallel brushing scenarios, the experimental tests show reduced amplitude and duration peaks during the inversion of the motion. This difference is localised and limited to a very small distance range. On the other hand, the assessment of both normal and tangential forces during the stable brushing phases can be considered accurate enough for engineering purposes.

Specifically, the phases of inversion of motion can be reviewed, focusing on the differences between experiments and models, which need to be deepened with a greater understanding of the phenomena of instability and buckling of the bristles. When a bristle in



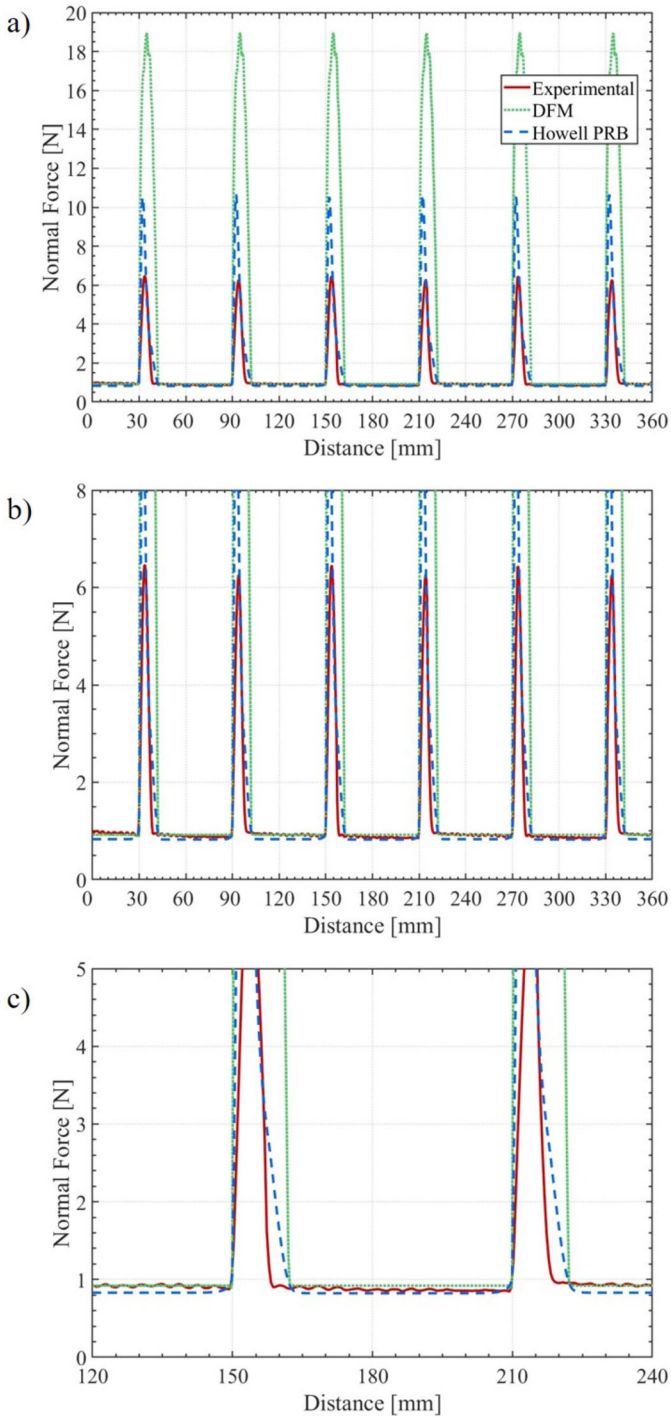


**Fig. 13** a) Comparison of the results obtained for the normal force about parallel brushing; b) comparison enlargement along the y-axis; c) comparison about a single period

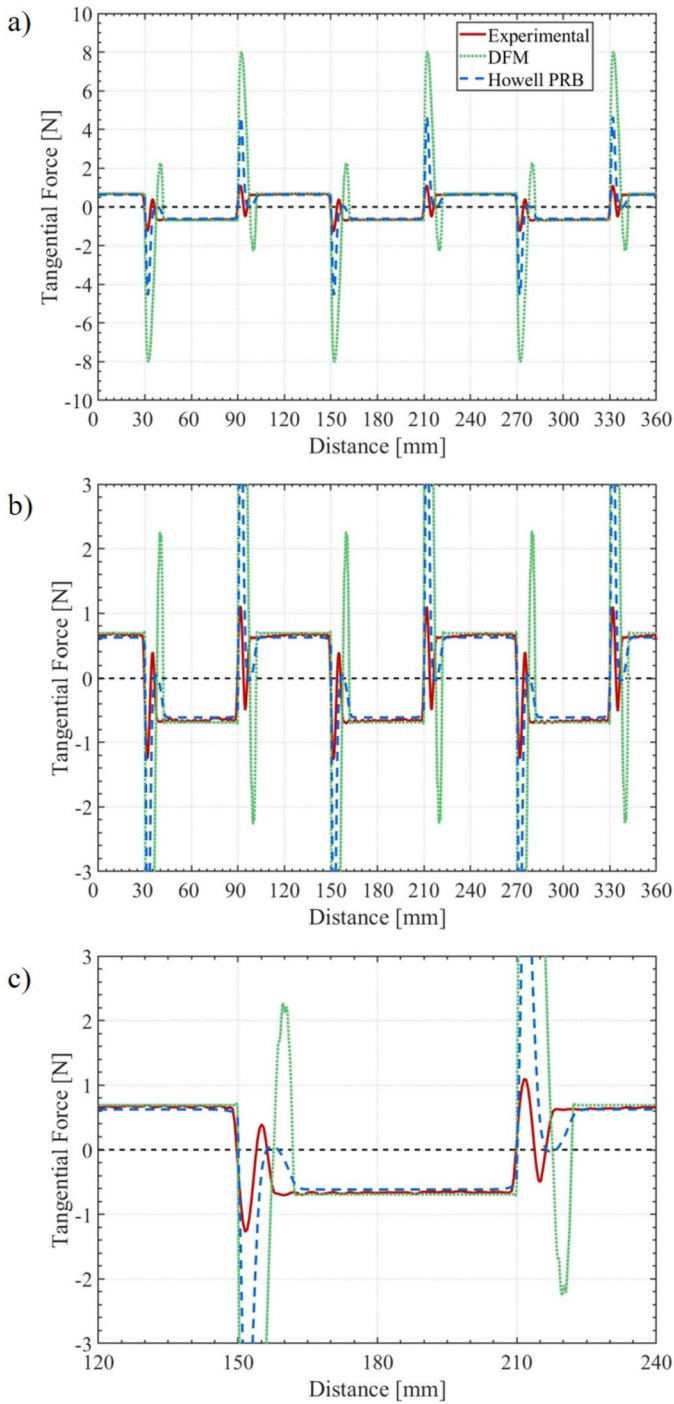


**Fig. 14** a) Comparison of the results obtained for the tangential force about parallel brushing; b) comparison enlargement along the y-axis; c) comparison about a single period

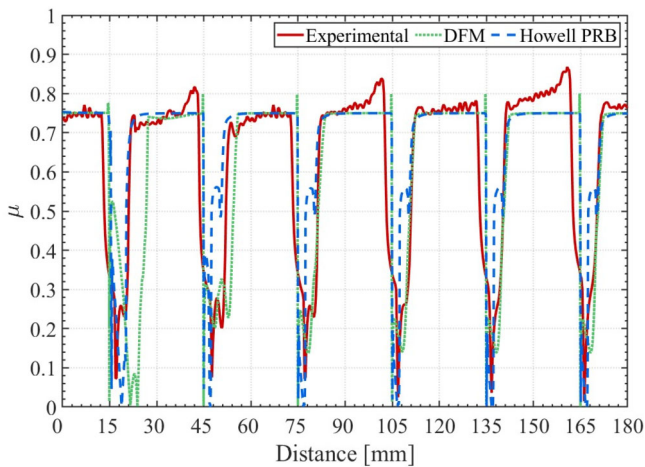


**Fig. 15** Comparison of the results obtained for the friction coefficient about orthogonal brushing

contact with a surface is dragged, it assumes a curved-line configuration with a constant sign curvature due to the moment generated by the contact force. At the point of motion inversion, the direction of the tangential contact force is reversed, and this change generates more configurations of equilibrium, depending on the contact-force amplitude. The deformed shape at the beginning of the inversion becomes unstable and tends to become stable, looking for a snap-through configuration. In the experiments, a more stable configuration is reached because of small misalignments outside the plane and unevenness of the contact forces. Both simulation models, due to the ideal geometries and boundary conditions, have difficulty in capturing this phenomenon and tend to overestimate the contact forces at the point of inversion because the bristles jam and delay the transition from an unstable configuration to a stable configuration. Additionally, due to jamming, this transition takes place through an intermediate configuration in which the neutral axis of the bristles has an inflexion and two opposite curvatures, which, as illustrated in the images in Fig. 10, may occur in the experiments but with fewer occurrences.

Figure 15 and Fig. 16 compare the obtained results concerning the friction coefficient in orthogonal and parallel brushing, respectively. The experimental tests exhibit a small variability of the friction coefficient due to the actual roughness of the flat surface and the compliance of the supports. Local increases of approximately 13% for orthogonal brushing and 11% for parallel brushing in the friction coefficient are evident, compared to the prescribed working conditions of the multibody models.

The obtained results seem to confirm the validity of both multibody models as effective tools for qualitatively and quantitatively capturing the behaviour of toothbrush bristles in contact with a flat surface during effective brushing, notwithstanding certain simplifying assumptions. However, in the context of motion reversals, the quantitative limitation arises from the assumption of neglecting mutual interaction effects among the bristles in the multibody models. Nevertheless, the trend of motion reversal and the deformation of the bristles faithfully align the experimental case.

Simulations have been conducted on an Intel I9 12900KF Workstation with 128 GB Ram. The comparisons between the computational time of both the PRBM and DFM approaches are reported in Table 3. The PRBM requires less computational time than the DFM in both

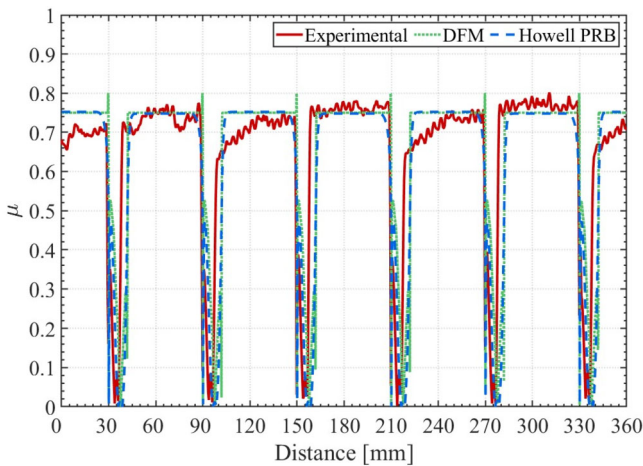


**Fig. 16** Comparison of the results obtained for the friction coefficient about parallel brushing

**Table 3** Computational time of the two approaches for the two scenarios

Model	Orthogonal brushing	Parallel brushing
<i>PRBM</i>	2474 s	4659 s
<i>DFM</i>	7354 s	7926 s

the scenarios. The PRBM can provide sufficient accuracy in terms of overall normal and tangential forces as discussed in the previous section; however, it has some limitations:

- the possibility of problems in contact detection during the change in the direction of motion;
- considering the visual comparison, the deformation of the bristles, especially during the inversion phases cannot be assessed with sufficient accuracy.

In contrast, despite the greater computational burden, DFM exhibits a higher accuracy in both visual-deformation and numerical-load comparisons, proving to be a more suitable and reliable modelling approach for such a complex problem.

From the discussion of the results, the PRBM and the DFM models show very good agreement with the experimental setup in the effective brushing zone. Although the DFM shows a smaller error compared to PRBM, even the error percentage of PRBM is negligible for engineering purposes. Additionally, looking at the computational time, the PRBM is faster than DFM. In both cases, the adoption of a three-dimensional model favours the estimation of the passages through snap-through configurations that occurs mainly with an out-of-plane deformation.

However, because of its simple discretisation, PRBM cannot describe the accurate deformation of the bristle during the inversion of motion. Consequently, in this phase, a lower accuracy in load prediction is observed.

## 6 Conclusions

This paper presents the development and comparative analysis of two multibody modelling approaches, namely the pseudo-rigid-body model and the discrete flexible model, aimed at assessing the contact forces exerted by toothbrush bristles on a flat surface during orthogonal and parallel brushing. Solutions are compared with an experimental setup to compare the accuracy of bristle deflection, evaluated through visual inspection, and that of the contact forces, evaluated numerically. The results reveal that both multibody models may assess contact-force values consistent with those derived from the experimental model during effective brushing. The three-dimensional modelling of bristles makes it possible to capture more accurately the snap-through phenomena of the deformed bristles in the phases of motion inversion. The PRB model, featuring a reduced computational burden due to a smaller number of rigid-body and mass–spring–damper components, exhibits affordable calculation times. The DFM model accurately captures the actual deformation of the bristles, while the PRB model roughly approximates the deformation observed in the experimental tests. In terms of contact force, the DFM model shows more accuracy compared to the PRB model. Neglecting the mutual interaction between the bristles did not affect the accuracy of the brushing results in terms of forces, but the inclusion of mutual interaction among bristles seems necessary to achieve a higher accuracy in the results in the motion-inversion phases when the bristles are mixed together. Generally, both models can be used to investigate case studies in which the brushing generates an out-of-plane motion of the bristles and in studies in which the shape, size or materials of the bristles are different, thus extending the proposed modelling approach also in situations of more complex dynamics.

**Acknowledgements** The authors wish to acknowledge the support of the National Center for HPC, Big Data and Quantum Computing, Project CN\_00000013 – CUP E83C22003230001, Mission 4 Component 2 Investment 1.4, funded by the European Union – NextGenerationEU.

**Author contributions** A.C. and L.D. implemented the numerical models. A.C. and M.C. designed and tested the experimental setup. M.M. provided the toothbrush sample and implemented the brushing procedure. P.P.V. and M.C. worked on the conceptualization of the study. P.P.V. acted as supervisor and coordinator of all the activities.

**Data Availability** No datasets were generated or analysed during the current study.

## Declarations

**Competing interests** The authors declare no competing interests.

## References

1. Bay, I., Kardel, K.M., Skougaard, M.R.: Quantitative evaluation of the plaque-removing ability of different types of toothbrushes. *J. Periodontol.* **38**, 526–533 (1967)
2. Gibson, J.A., Wade, A.B.: Plaque removal by the bass and roll brushing techniques. *J. Periodontol.* **48**, 456–459 (1977)
3. Robinson, H.B.G.: Toothbrushing habits of 405 persons. *J. Am. Dent. Assoc.* **33**, 1112–1117 (1946)
4. Van der Weijden, G.A., Timmerman, M.F., Danser, M.M., Van der Velden, U.: Relationship between the plaque removal efficacy of a manual toothbrush and brushing force. *J. Clin. Periodontol.* **25**, 413–416 (1998)
5. Van der Weijden, G.A., Timmerman, M.E., Nijboer, A., Lie, M.A., van der Veiden, U.: A comparative study of electric toothbrushes for the effectiveness of plaque removal in relation to toothbrushing duration—time study. *J. Clin. Periodontol.* **20**, 476–481 (1993)

6. Rawls, H.R., Mkwayi-Tulloch, N.J., Krull, M.E.: A mathematical model for predicting toothbrush stiffness. *Dent. Mater.* **6**, 111–117 (1990)
7. Kaiser, E., Meyners, M., Markgraf, D., Stoerker, U., Koppenfels, R., Adam, R., Soukup, M., Wehrbein, H., Erbe, C., et al.: Brush head composition, wear profile, and cleaning efficacy: an assessment of three electric brush heads using in vitro methods. *J. Clin. Dent.* **25**, 19–25 (2014)
8. Langa, G.P.J., Muniz, F.W.M.G., Wagner, T.P., Silva, C.F., Rösing, C.K.: Anti-plaque and anti-gingivitis efficacy of different bristle stiffness and end-shape toothbrushes on interproximal surfaces: a systematic review with meta-analysis. *J. Evid.-Based Dent. Pract.* **21**, 101–148 (2021)
9. Heath, J.R., Wilson, H.J.: Classification of toothbrush stiffness by a dynamic method. *Br. Dent. J.* **130**, 59–66 (1971)
10. Organization, I.S.: Dentistry-Stiffness of the Tufted Area of Toothbrushes. Standards Document ISO **8627** (1987)
11. Stango, R.J., Cariapa, V., Prasad, A., Liang, S.-K.: Measurement and analysis of brushing tool performance characteristics, part 1: stiffness response (1991)
12. Cariapa, V., Stango, R.J., Liang, S.-K., Prasad, A.: Measurement and Analysis of Brushing Tool Performance Characteristics, Part 2: Contact Zone Geometry (1991)
13. Heinrich, S.M., Stango, R.J., Shia, C.Y.: Effect of workpart curvature on the stiffness properties of circular filamentary brushes (1991)
14. Lei, B., Ziqi, M., Jinyang, L., Caishan, L.: Dynamic modelling and analysis for a flexible brush sampling mechanism. *Multibody Syst. Dyn.* **56**(4), 335–365 (2022)
15. Ziqi, M., Zhuyong, L., Huaiwu, Z., Jinyang, L.: Dynamic modeling and analysis of satellite detumbling using a brush type contactor based on flexible multibody dynamics. *Mech. Mach. Theory* **170**, 104–675 (2022)
16. Shia, C.-Y., Stango, R.J., Heinrich, S.M.: Analysis of contact mechanics for a circular filamentary brush/workpart system (1998)
17. Uhlmann, E., Sommerfeld, C.: Dynamic contact analysis of abrasive filaments with a discrete system. In: Proceedings of the 20th International Symposium on Advances in Abrasive Technology (2017)
18. Uhlmann, E., Sommerfeld, C.: Three-dimensional dynamic contact analysis of abrasive filaments with a multi-body system. *Proc. CIRP* **72**, 615–621 (2018)
19. Ma, Z., Liu, Z., Zou, H., Liu, J.: Dynamic modeling and analysis of satellite detumbling using a brush type contactor based on flexible multibody dynamics. *Mech. Mach. Theory* **170**, 104675 (2022)
20. Howell, L.L.: Compliant mechanisms. In: 21st Century Kinematics: The 2012 NSF Workshop (2013)
21. Yu, Y.-Q., Howell, L.L., Lusk, C., Yue, Y., He, M.-G.: Dynamic modeling of compliant mechanisms based on the pseudo-rigid-body model (2005)
22. Valentini, P.P., Pennestrì, E.: Modeling elastic beams using dynamic splines. *Multibody Syst. Dyn.* **25**, 271–284 (2011)
23. Cirelli, M., Cellupica, A., D’Angelo, L., Mazur, M., Valentini, P.P.: Numerical and machine-aided experimental models for simulating the 3D compliance of a toothbrush. *Machines* **11**, 783 (2023)
24. Cellupica, A., D’Angelo, L., Cirelli, M., Mazur, M., Valentini, P.P.: Multibody approach to model toothbrush bristles elasto-kinematics. In: Proceedings of the ECCOMAS Thematic Conference on Multibody Dynamics, Lisbon, Portugal (2023)
25. Mazur, M., Ottolenghi, L., Scrascia, A., Cera, M., Cirelli, M., Valentini, P.P.: Sub-structured flexible multibody model for simulating toothbrush cleaning process. In: *Archive of Applied Mechanics*. In Press (2023)
26. Cheli, F., Pennestrì, E., et al.: *Cinematica e Dinamica dei Sistemi Multibody*, vol. 2. CEA Casa Editrice Ambrosiana (2009)
27. Huston, R.L., Wang, Y.: Flexibility effects in multibody systems. In: *Computer-Aided Analysis of Rigid and Flexible Mechanical Systems*, pp. 351–376 (1994)
28. Hutchinson, J.R.: Shear coefficients for Timoshenko beam theory. *J. Appl. Mech.* **68**, 87–92 (2001)
29. Bauchau, O.A., Han, S.: Advanced beam theory for multibody dynamics. In: *International Design Engineering Technical Conferences and Computers and Information in Engineering Conference* (2013)
30. Rasmussen, N.O., Wittwer, J.W., Todd, R.H., Howell, L.L., Magleby, S.P.: A 3d pseudo-rigid-body model for large spatial deflections of rectangular cantilever beams. In: *International Design Engineering Technical Conferences and Computers and Information in Engineering Conference* (2006)
31. Cera, M., Cirelli, M., Colaiacovo, L., Valentini, P.P.: Second-order approximation pseudo-rigid model of circular arc flexure hinge. *Mech. Mach. Theory* **175**, 104963 (2022)
32. Valentini, P.P., Pennestrì, E.: Elasto-kinematic comparison of flexure hinges undergoing large displacement. *Mech. Mach. Theory* **110**, 50–60 (2017)
33. Pennestrì, E., Rossi, V., Salvini, P., Valentini, P.: Review and comparison of dry friction force models. *Nonlinear Dyn.* **83**(4), 1785–1801 (2016)

34. Choi, J., Ryu, H.S., Kim, C.W., Choi, J.H.: An efficient and robust contact algorithm for a compliant contact force model between bodies of complex geometry. *Multibody Syst. Dyn.* **23**, 99–120 (2010)
35. Young, W.C., Budynas, R.G., Sadegh, A.M.: *Roark's Formulas for Stress and Strain*. McGraw-Hill, New York (2012)
36. Popov, V.L., et al.: *Contact Mechanics and Friction*. Springer, Berlin (2010)
37. Flores, P., Machado, M., Silva, M.T., Martins, J.M.: On the continuous contact force models for soft materials in multibody dynamics. *Multibody Syst. Dyn.* **25**, 357–375 (2011)
38. Choi, J., Rhim, S., Choi, J.H.: A general purpose contact algorithm using a compliance contact force model for rigid and flexible bodies of complex geometry. *Int. J. Non-Linear Mech.* **53**, 13–23 (2013)
39. Wu, S.C., Yang, S.M., Haug, E.J.: Dynamics of mechanical systems with Coulomb friction, stiction, impact and constraint addition-deletion. *Mech. Mach. Theory* **21**(5), 417–425 (1986)
40. Cha, H., Choi, J., Ryu, H., Choi, J.: Stick-slip algorithm in a tangential contact force model for multi-body system dynamics. *J. Mech. Sci. Technol.* **25**, 1687–1694 (2011)
41. Pennestrì, E., Rossi, V., Salvini, P., Valentini, P.P.: Review and comparison of dry friction force models. *Nonlinear Dyn.* **83**(4), 1785–1801 (2015)
42. Autiero, M., Cera, M., Cirelli, M., Pennestrì, E., Valentini, P.P.: Review with analytical-numerical comparison of contact force models for slotted joints in machines. *Machines* **10**, 966 (2022)

**Publisher's Note** Springer Nature remains neutral with regard to jurisdictional claims in published maps and institutional affiliations.

Springer Nature or its licensor (e.g. a society or other partner) holds exclusive rights to this article under a publishing agreement with the author(s) or other rightsholder(s); author self-archiving of the accepted manuscript version of this article is solely governed by the terms of such publishing agreement and applicable law.

## Authors and Affiliations

Alessio Cellupica<sup>1</sup> · Luca D'Angelo<sup>1</sup> · Marco Cirelli<sup>1</sup> · Marta Mazur<sup>2</sup> · Pier Paolo Valentini<sup>1</sup>

✉ P.P. Valentini  
[valentini@ing.uniroma2.it](mailto:valentini@ing.uniroma2.it)

A. Cellupica  
[alessio.cellupica@uniroma2.it](mailto:alessio.cellupica@uniroma2.it)

L. D'Angelo  
[luca.d.angelo@uniroma2.it](mailto:luca.d.angelo@uniroma2.it)

M. Cirelli  
[marco.cirelli@uniroma2.it](mailto:marco.cirelli@uniroma2.it)

M. Mazur  
[marta.mazur@uniroma1.it](mailto:marta.mazur@uniroma1.it)

<sup>1</sup> Department of Enterprise Engineering, University of Rome Tor Vergata, Via del Politecnico 1, 00133, Rome, Italy

<sup>2</sup> Department of Dental and maxillo-facial Sciences, University of Rome La Sapienza, Piazzale Aldo Moro 5 00185, Rome, Italy